Mechanical behaviour of welded high strength steel rectangular hollow section joints

Xin, Haohui; Kisoensingh, Prishilla; Veljkovic, Milan

DOI
10.1016/j.engfailanal.2021.105410

Publication date
2021

Document Version
Final published version

Published in
Engineering Failure Analysis

Engineering Failure Analysis 125 (2021) 105410

Contents lists available at ScienceDirect

Engineering Failure Analysis

journal homepage: www.elsevier.com/locate/engfailanal

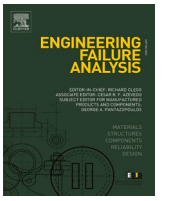

Mechanical behaviour of welded high strength steel rectangular hollow section joints

Haohui Xin [a,b,*], Prishilla Kisoensingh [b], Milan Veljkovic [b]

[a] Department of Civil Engineering, School of Human Settlements and Civil Engineering, Xi'an Jiaotong University, Xi'an, China[1]
[b] Faculty of Civil Engineering & Geosciences, Delft University of Technology, 2628 CD Delft, Netherlands[2]

ARTICLE INFO

Keywords:
Rectangular hollow section joints
High-strength steels
Ultimate capacity
Material reduction factor

ABSTRACT

The material reduction factor of rectangular hollow section (RHS) joints in a new version of Eurocode 3 part 1–8 is validate for steel with the nominal yield strength up to 700 MPa. In this paper, finite element simulations of gap K-joints are conducted to investigate effects of material properties, gap size of the joint, the brace to chord width ratio and welds type on the secondary bending stresses and the resistance. The governing failure mode considered for all the FE models is the chord face failure followed by brace sidewall failure. The ratio of axial stresses to the nominal stress was lower in the compressive brace made of higher strength steel grades compared to the mild strength grades. The maximum secondary bending stresses is 0.12–0.32 yield strength. The secondary bending stresses are increasing with the increase of the steel grade and the brace to chord width ratio and with reducing the gap size. The level of secondary bending stresses varied between 38% and 56% of the average normal axial stress. The secondary bending stresses of fillet-welded joints are larger than the butt-welded joints. The yield line model is used to predict the ultimate load and good agreement is obtained compared with FE results.

1. Introduction

The high strength steel (HSS) benefits long-span and high-rise structures in civil engineering sector, such as sports arenas and bridges [1–5]. Tubular structures are generally recommended for such high-rise and long-span structures [6]. The safety and reliability of HSS welded hollow section joints are very important to tubular structures [7]. The hollow section joints could be divided into circular hollow section (CHS) joints [8–10] and rectangular hollow section (RHS) joints [13,14].

One obstacle for competitive use in engineering practice is due to uncertainties in whether current design standards of rectangular hollow section (RHS) joints validated for mild strength steels can be used to HSSs [15]. Because of non-uniform stiffness, eccentric forces and the large deformations in a truss girder, secondary bending stresses generally occurred in the tubular joints. In the design of truss structures, the joints are generally simplified as pinned jointed braces and continuous chords [7]. Bjork et al. [16] showed that the secondary bending moment is highly dependent on the joint geometry and material properties. Their results showed that the secondary bending stresses requires additional attention if high strength steels are used. The secondary bending moment is dependent on the plastic moment capacity of the brace member or the joints. The trilinear stress-strain relationship without softening or damage in their

* Corresponding author.
E-mail address: xinhaohui@xjtu.edu.cn (H. Xin).
[1] Present.
[2] Previous.

https://doi.org/10.1016/j.engfailanal.2021.105410
Received 25 September 2020; Received in revised form 22 March 2021; Accepted 29 March 2021
Available online 5 April 2021

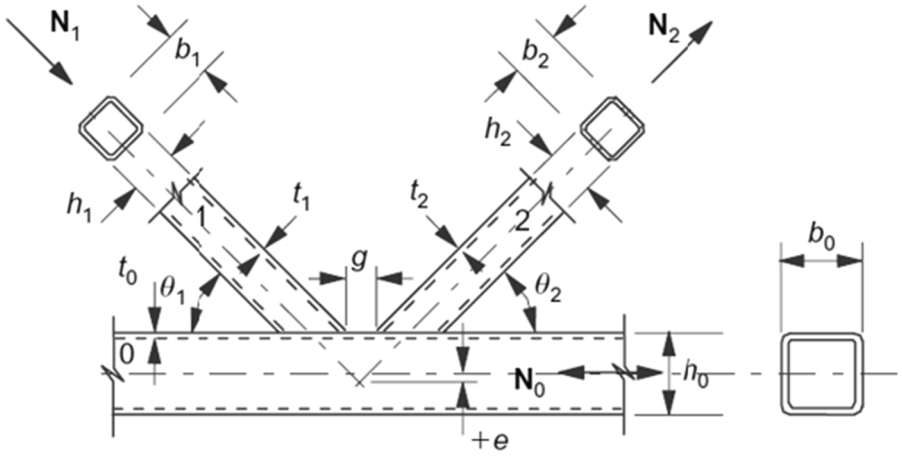

Fig. 1. Gap K-joint parameters.

Table 1
Joint geometry for the parametric study.

Joint layout	b_o (mm)	t_o (mm)	b_i (mm)	t_i (mm)	g (mm)	θ_i (°)	e (mm)	β (-)	Weld Type
K1	120	5	80	5	40	30	−2.3	0.67	Fillet
K2	120	5	80	5	25	30	−6.6	0.67	Fillet
K3	140	6.3	70	5	40	30	−18	0.50	Fillet
K4	140	6.3	80	5	40	30	−12.3	0.57	Fillet
K5	140	6.3	90	5	40	30	−5.5	0.67	Fillet
K6	140	6.3	70	5	40	30	−18	0.50	Butt
K7	140	6.3	80	5	40	30	−12.3	0.57	Butt
K8	140	6.3	90	5	40	30	−6.5	0.53	Butt

Table 2
The weld width, t_w, used in FEA.

Steel grade	Weld size	
$F_y \leq 500$ MPa	$t_w \geq 1.4t_i$	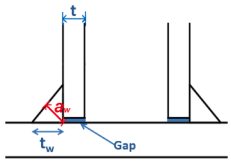
500 MPa $< F_y <$ 700 MPa	$t_w \geq 1.69t_i$	
700 MPa $< F_y \leq$ 960 MPa	$t_w \geq 1.98t_i$	

finite element simulation may lead to an unreal increase of secondary bending moment especially when the local material is in the stage of the post necking or fracture. The European design code [15] neglects the secondary bending stresses, and is validate for the RHS joints made of the steel with the nominal yield strength up to 460 MPa. A new draft version of European standard part 1–8 chapter 9 [17] proposes design rules for RHS joints with a yield strength up to 700 MPa. The design rules, which were originally developed by CIDECT [18], are based on experimental, numerical and analytical analysis and validated for a range of parameters for steel grades up to S460. The validity range gives various limitations on geometrical parameters of joints to ensure that the members and the joints have sufficient resistance validated by the design resistance formula. An open question on what would be justified level of material factors necessary to accept.

The behavior of hollow section joint may be different with increasing steel nomial yield strength and must be therefore checked. In this paper an attempt is made to investigate the effect of the secondary bending stresses of RHS joints with four steel grades, two gap size, three braces width to chord width ratios (β) and two types of welds. A parametric study is performed on the gap K-joint made of square hollow sections using finite element analysis.

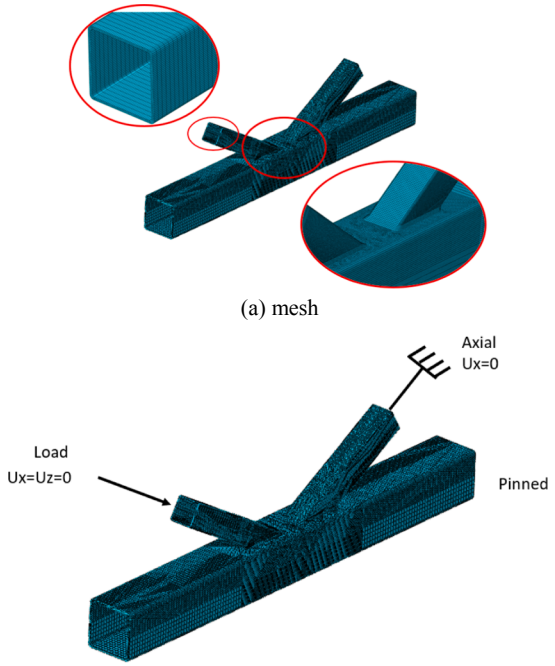

(a) mesh

(b) Boundary conditions

Fig. 2. Finite element mesh and boundary conditions of the K joint.

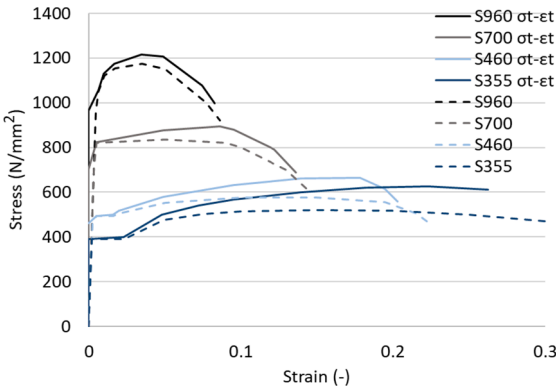

Fig. 3. Nominal and true stress-strain relationship.

2. Finite element model

2.1. Geometry

Fig. 1 presented the symbols of the gap K-joint and Table 1 listed the values of each symbol. The angles between the brace and chord are same, $\theta i = 30^{\circ}$. β denoted the brace width to chord width ratio. Two gap size of $G_0 = 25$ mm and $G_1 = 40$ mm, three braces to chord width ratios of $\beta_1 = 0.50$, $\beta_2 = 0.57$ and $\beta_3 = 0.67$, fillet and butt welds are varied to investigate their effects on the secondary bending stresses and the failure modes. The weld width t_w of fillet welds is related to the brace thickness and the yield strength of the material, as listed in Table 2.

2.2. Mesh and boundary conditions

C3D8 element of ABAQUS is used to model the K-joints and welds. The mesh and boundary conditions are shown in Fig. 2. As shown in Fig. 2b, one end of the chord is pinned, and the other end is left free. One brace member is pinned, and the other brace member is roller pinned to allow the translation in the axial direction. MPC constrain is used to transfer the load from the referemce point to the

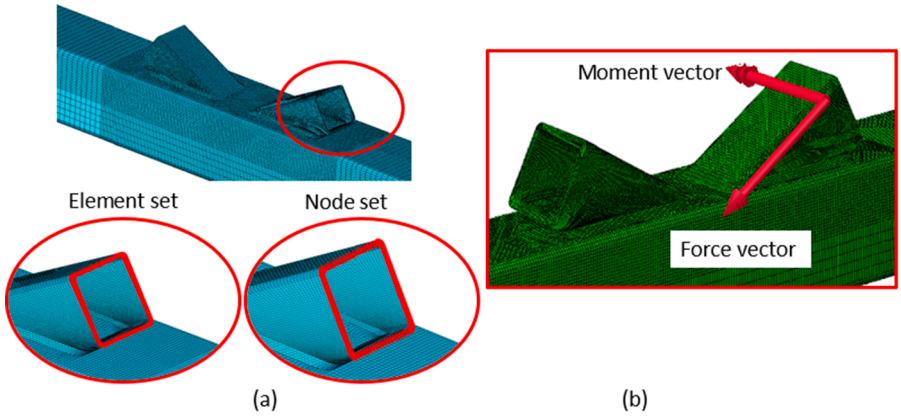

Fig. 4. (a) Element set and node set and (b) moment and force vector K-joint.

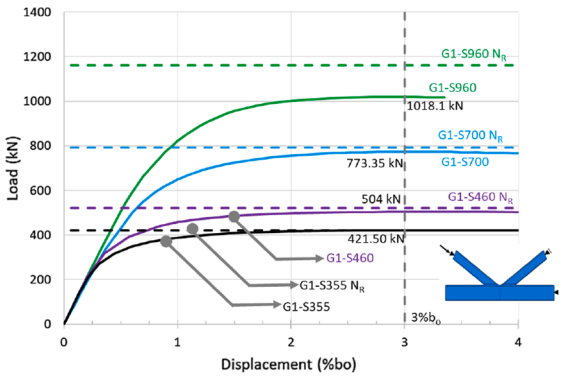

Fig. 5. Load-displacement of K1 joints with different steel grades.

Table 3
Comparisions between FE results and design resistance with different steel grades.

Model	N_{FEA} (kN)	N_R (kN)	N_R/N_{FEA} (-)	$N_{R,Cf}/N_{FEA}$ (-)
K1-S355	421.49	420.69	1.00	1.00
K1-S460	503.99	522.17	1.04	0.93
K1-S700	773.35	792.41	1.02	0.82
K1-S960	1018.81	1162.36	1.14	0.91

brace member.

2.3. Material parameters

Material data obtained from a set of coupon specimens in RUOSTE project are used in the FEA [6]. The stress-strain curves for the steel grade varying from S355 to S960 are shown in Fig. 3 [19]. It should be noted that ratio of yield strength to tensile strength is 0.75 for S355, 0.80 for S460, 0.84 for S700, and 0.82 for S960.

2.4. Secondary bending moment

As shown in Fig. 4, the secondary bending moment is defined as the stress integration at the cross section 95 mm away from top chord surface at the compression brace. The secondary bending stress σ_m is calculated based on FE secondary bending moment and moment inertia. The average stress or nominal stress σ_n is determined using the obtained FE axial force and the cross-sectional area.

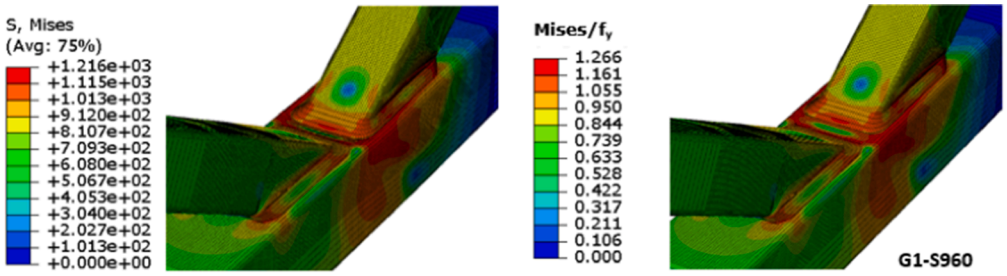

(a) S960

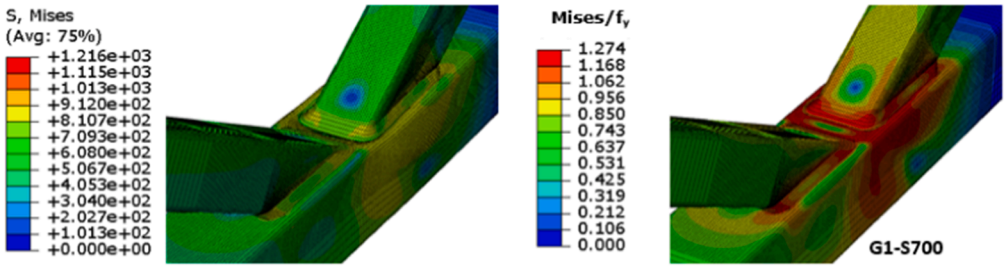

(b) S700

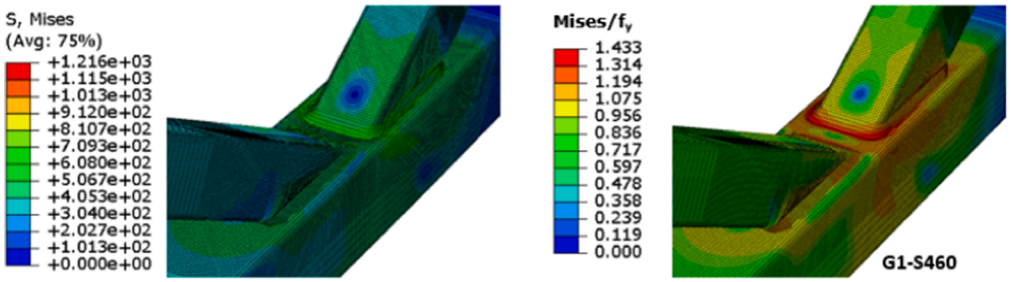

(c) S460

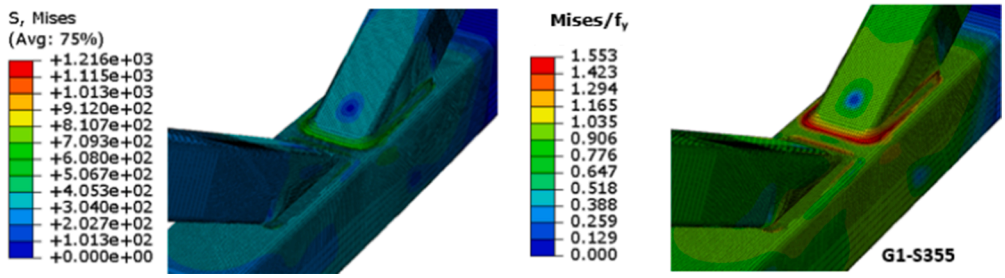

(d)S355

Fig. 6. Mises stresses distribution of of K1 joints with different steel grades.

3. Parametric analysis

3.1. *Effects of steel grades*

Fig. 5 shows the load-displacement relationship of K1 joints with different steel grades. Table 3 listed the comparisions between FE simulation results and design resistance [17] with different steel grades. The joints presented chord face failure (CFF). The design

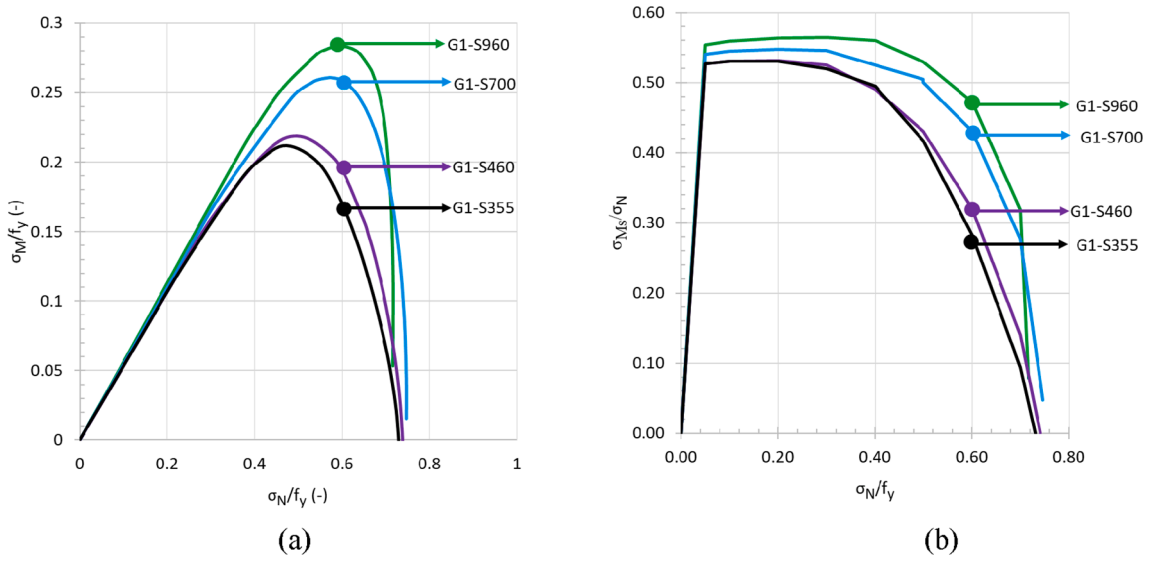

Fig. 7. Secondary bending stress and the level of secondary bending stress for K1 joints with different steel grades.

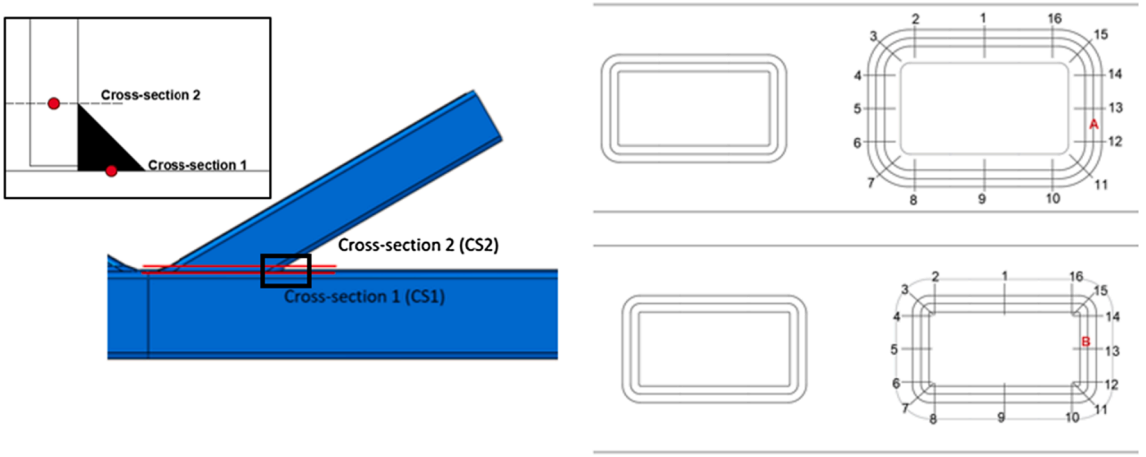

Fig. 8. Positions of cross-sections for K1 joints.

resistance without considering reduction of material factor (C_f) and the partial safety factor denoted as N_R, and the design resistance only considering the material factor (C_f) [17] denoted as $N_{R,CF.}$ The load corresponding to the 3%b_0 (b_0 is the width of the chord) deformation limit is considered as the ultimate load of the joints. The ultimate load of RHS joints made of S460, S700, and S960 is 20%, 83% and 142% larger than it of RHS joints made of S355. The ultimate load from FE is 14%, 2% and 4% larger than the recommended design load of Eurocode [17]. Based on the FE results, the reduction factor is determined to be 1.0, 0.9, 0.8 and 0.8 for the RHS joints made of S355, S460, S700 and S960.

The stress distribution at 3%b_0 deformation is shown in Fig. 6. The governing failure mode for all FE models is the chord face failure. In the zone of welds, the stresses are higher than the nominal yield strength of base materials. The ratio of maximum mises stress to nominal yield strength is 1.55, 143, 1.27 and 1.27 for the steel grades S355, S460, S690 and S960 respectively. That is the ratio of maximum mises stress to nominal yield strength is lower for the joints made of high steel grades.

In terms of K1 joints with different steel grades, the relationship between the ratio σ_m/f_y and the ratio σ_n/f_y is shown in Fig. 7a, and the relationship between the ratio σ_m/σ_n and the ratio σ_n/f_y is presented in Fig. 7b. The secondary stress firstly increased and later decreased with the increasing applied load. The ratio σ_m/f_y is larger with the nominal yield strength increasing. The ratio σ_m/σ_n decreased with the increasing applied load.

As shown in Fig. 8, two cross-sections are selected to show the stress distribution along the brace. Figs. 9 and 10 the axial stress distribution at the design resistance in position 2–8 and 10–16 in the middle line of both the cross sections. The compressive axial stresses in the joint are larger than the nominal yield strength. The combination of secondary bending stress and the average stress at 3%b_0 deformation is also plotted in the figures The axial stress ratio between local stress and the average stress is largest for K-joints

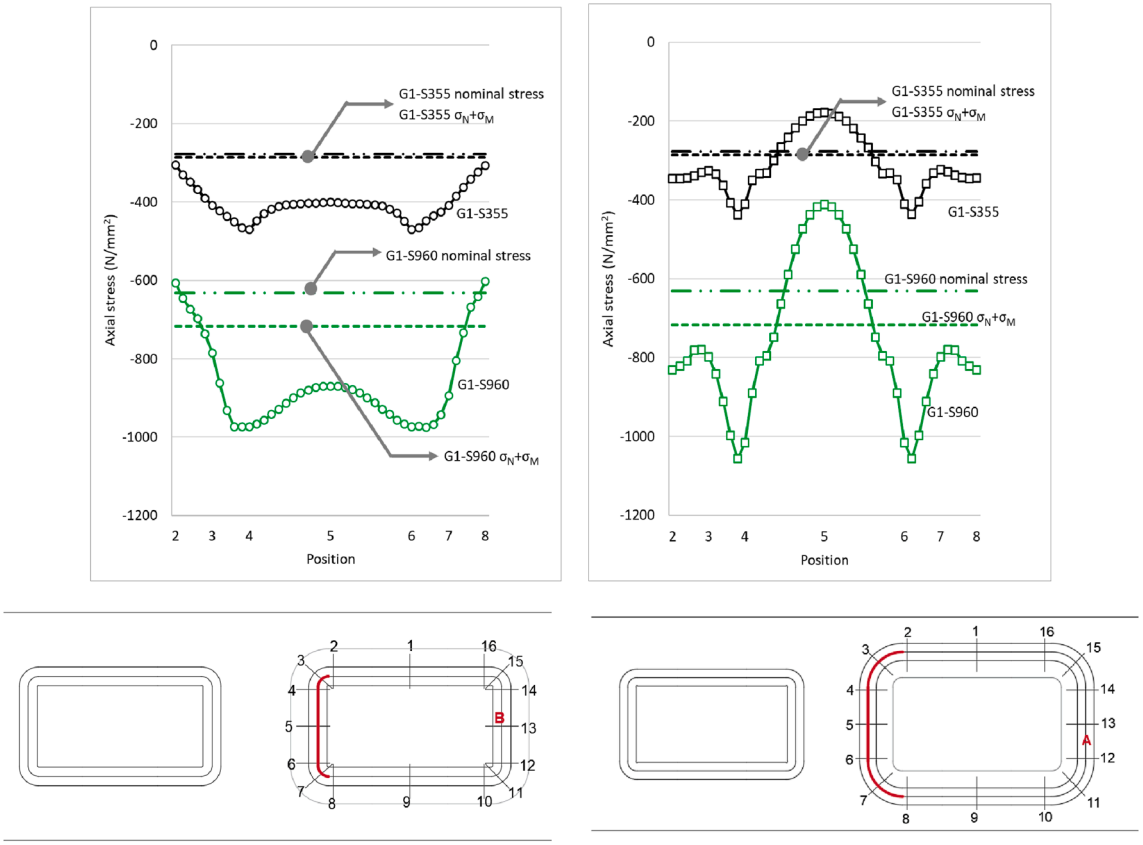

Fig. 9. Stress distribution of K1 joint in position 2–8 (a)cross-section 1 and (b) cross-section 2.

made of S355 materials and lowest for K-joints made of S960 materials.

3.2. Effects of the gap size

Fig. 11 presented the load displacement curve for the joints with different gap sizes. Table 4 shows the comparisions between FE simulation results and design resistance [17] with different steel grades. The gap size has larger effects on the ultimate load of K-joints made of mild steel. The joint made of S355 with lower gap size G0 has 6% larger ultimate load resistance compared with the joint with gap size G1. Similarly, above ratio is 6%, 9% and 12% respectively for the joint made of S460, S700 and S960 respectively. The ultimate load of K joints with larger gap size from FE is 2%-14% larger than the ultimate load N_R based on Eurocode [17]. The ultimate load of K joints with smaller gap size is smaller or equal to the ultimate load N_R based on Eurocode [17].

The secondary bending stresses σ_m are higher for the K joints with smaller gap size with the same steel grade, as shown in Fig. 12. The σ_m for the K joints with smaller gap size is 7–15% larger. Maximum σ_m/σ_n ratio is around 53–56% for K-joint with larger gap size (G1) and 50–54% for K-joint with lower gap size (G0). The ratio σ_m/σ_n for the joint with gap size G1 is 5% larger compared to the joint with gap size G0. In general, the ratio σ_m/σ_n reached the top when the average stresses is up to $0.4f_y$ – $0.7f_y$.

3.3. Effects of the brace width to chord width ratio

To study the effect of the brace width to chord width ratio β on the high-strength hollow section joints, K-joints with three different β value are used. β1 denoted K3 joint, β2 denoted K4 joint, and β3 denoted K5 joint in Table 1. As shown in Fig. 13 and Table 5, the ultimate load of K-joint with ratio β_2 and β_3 is 15–18% and 34–40% larger than it of K-joint with β_1. Generally, the ultimate load is larger with the larger β value for the K-joint made of the same steel grade. However, the effect of the ultimate load of the β-value on high-strength joints are lower compared to it of the joints made of mild-strength steels.

As shown in Figs. 14 and 15, the β value effect on secondary bending stresses σ_m of K-joints made of high-strength steel is lower than it of K-joints made of mild strength steel. The σ_m is around $0.09fy$ – $0.19fy$ for K-joints made of high-strength steel. In general, K joints made of high-strength steel and with larger β value will lead to a larger σ_m when the force reached to the ultimate load. The ratio σ_m/σ_n of K joints with β_2 is 10%-13% larger than it with β_1, and the ratio σ_m/σ_n of K joints with β3 is 20–23% larger than it with β_1. For K-joints made of high-strength steel with same steel grade, larger β-value will lead to larger σ_m/σ_n ratio.

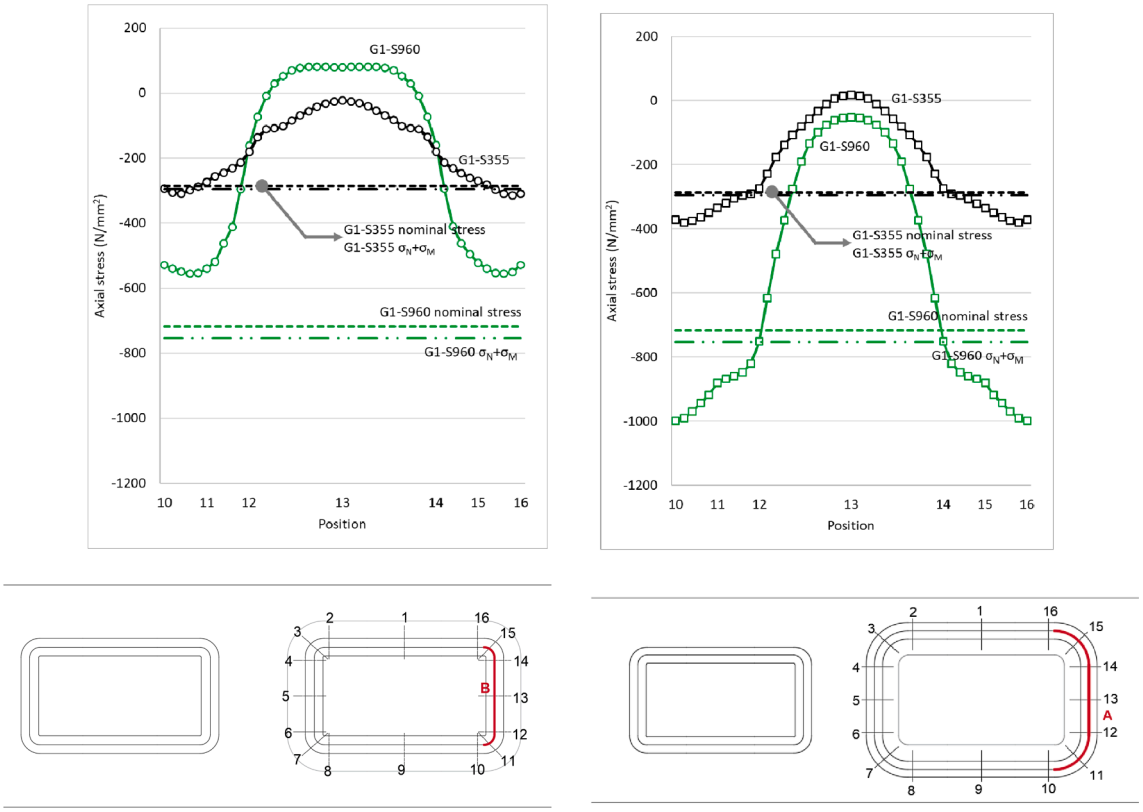

Fig. 10. Stress distribution of K1 joint in cross-section 1 and 2 in the positions 10–16.

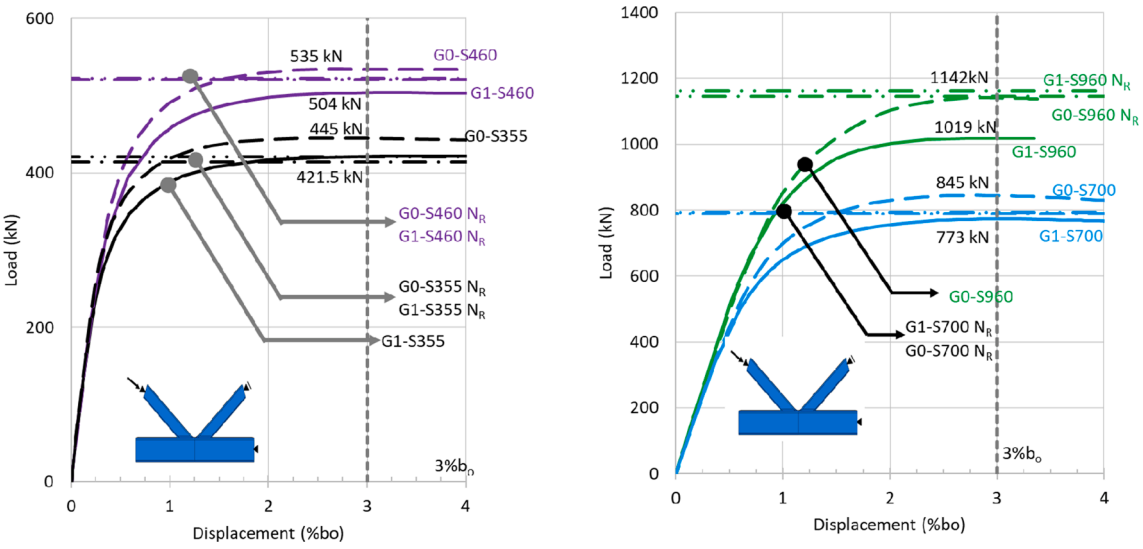

Fig. 11. Load displacement relation for two gap sizes, (G1 denoted K1 joint, G0 denoted K2 joint).

Table 4
Comparisions between FE results and design resistance with different gap size.

Model	N_{FEA} (kN)	N_R (kN)	N_R/N_{FEA} (-)	$N_{R,Cf}/N_{FEA}$ (-)
G0-S355	445.11	414.48	0.93	0.93
G0-S460	534.74	520.92	0.97	0.88
G0-S700	845.17	790.14	0.93	0.75
G0-S960	1141.92	1144.66	1.00	0.80
G1-S355	421.49	420.69	1.00	1.00
G1-S460	503.99	522.17	1.04	0.93
G1-S700	773.35	792.41	1.02	0.82
G1-S960	1018.81	1162.36	1.14	0.91

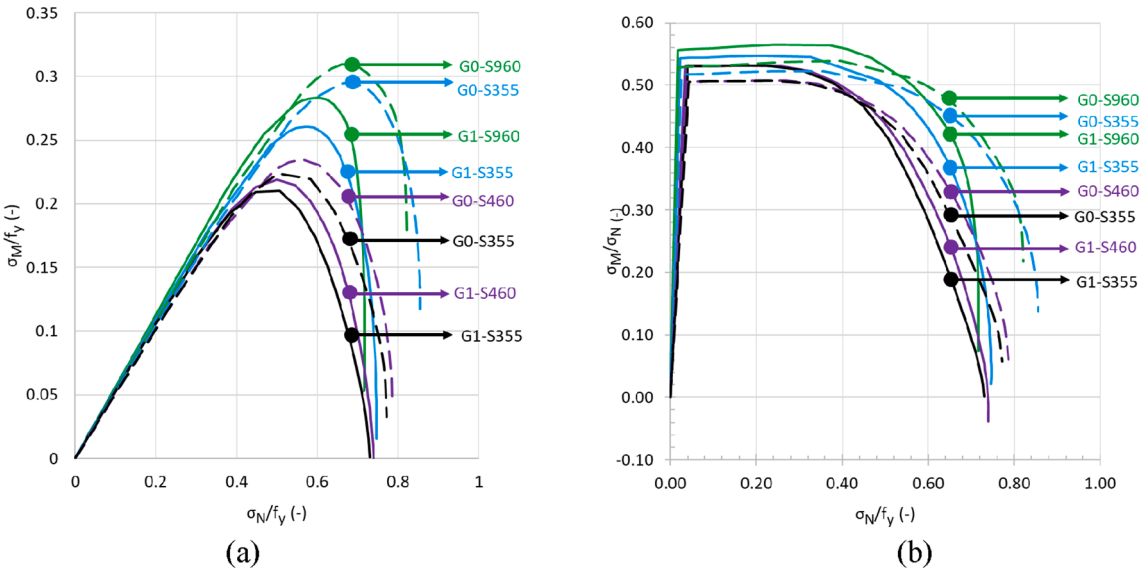

Fig. 12. Secondary bending stress and the level of secondary bending stress for K1 and K2 joints with different gap sizes.

3.4. Effects of weld types

The load-displacement curves with different weld types are plotted in Figs. 16–18. In terms of joints with the ratio β_1 (K3 and K6 joints in Table 1 coresponds to fillet and butt welds respectively), the K joint with fillet-welds result in 37%, 28%, 20% and 18% larger ultimate load when compared with K joint with butt-welds for S960, S700, S460 and S355 steel grades respectively. In terms of joints with the ratio β_2 (K4 and K7 joints in Table 1 coresponds to fillet and butt welds respectively), the K joint with fillet-welds result in 33%, 26%, 17% and 17% larger ultimate load when compared with K joint with butt-welds for S960, S700, S460 and S355 steel grades respectively. In terms of joints with the ratio β_2 (K4 and K7 joints in Table 1 coresponds to fillet and butt welds respectively), the K joint with fillet-welds result in 30%, 26%, 18% and 16% larger ultimate load when compared with K joint with butt-welds for S960, S700, S460 and S355 steel grades respectively.

As show in Figs. 19–21, the secondary bending stresses of K-joint made of fillet-welds are larger than it of K-joint made of butt-welds in terms of same steel grade. In detail, 37%, 38%,46% and 60% larger maximum secondary bending stress is observed for the K-joint made of S355, S460, S700 and S960 respectively. The maximum σ_m/σ_n ratio in the fillet-welded joints is 5–8% larger when compared to the butt-welded joints.

4. Yield line model

In this section, an attempt is done to predict the join resistance with the help of yield line mechanism analysis. This is done by equating the internal work and the external work. Deformation pattern of joint at ultimate load resistance are used to access the yield lines. The governing failure mode for the square hollow section joints is the chord face plastification, therefore the axial stress distribution in the chord are evaluated. It is observed that the stress at the chord face is non-uniformly distributed and along the brace perimeter the largest. Along the yield lines in the chord face, stresses are equal to the yield strength as shown in Fig. 22. As shown in Fig. 23, yield lines are assumed to be straight and generally appear at the brace toe and heel. The length of the yield lines is measured using the tool "path". The external work is equal to the joint resistance multiplied by a small deflection of the chord face. The displaced, rotated yield lines and the plastic moment are used to determine the internal work. The joint resistance is determined by dividing the

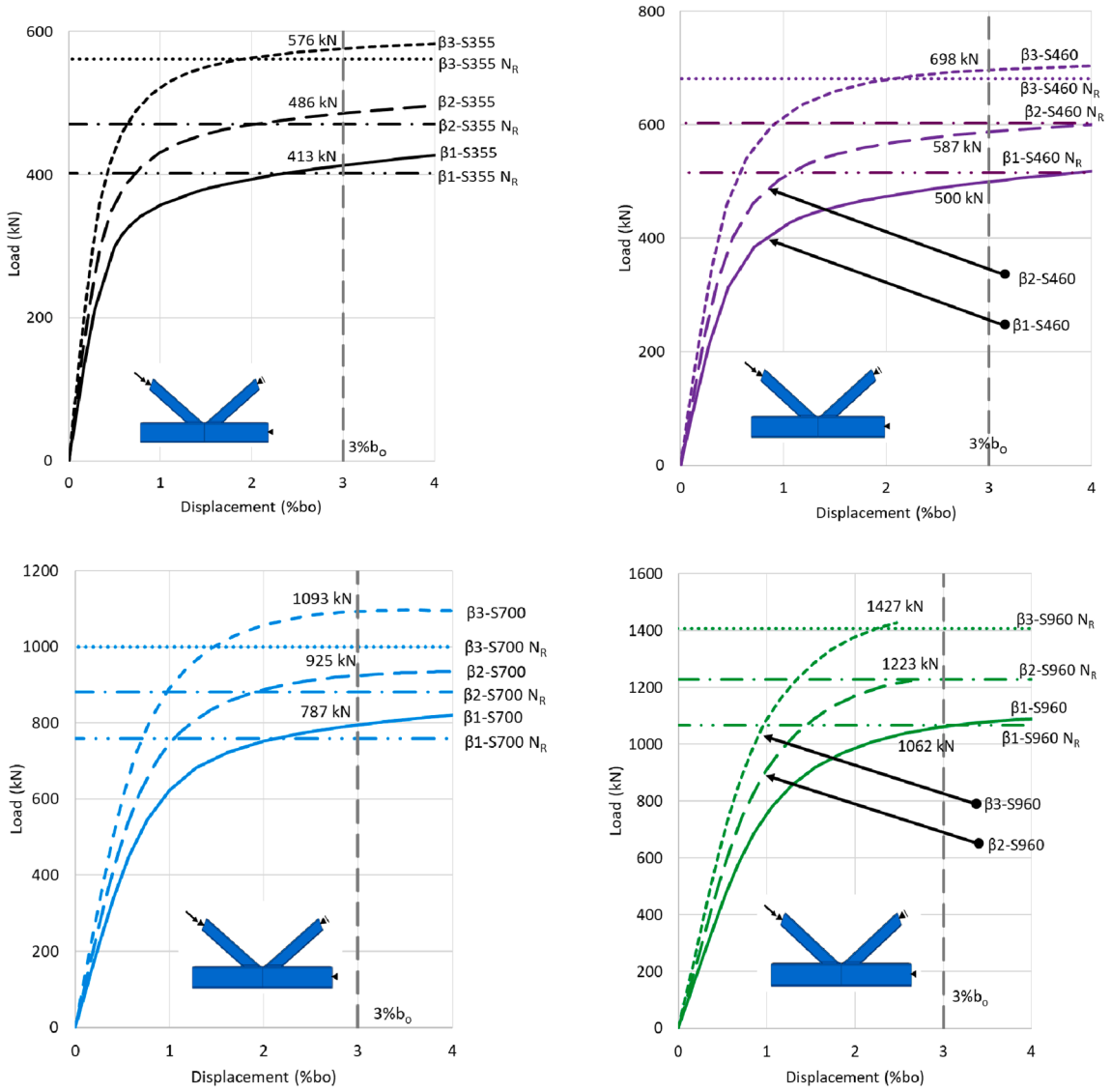

Fig. 13. Load displacement curve with different β for (a) S960, (b) S700, (c) S460 and (d) S355.

Table 5
Comparisions between FE results and design resistance with different β parameter.

Model	N_{FEA} (kN)	N_R (kN)	N_R/N_{FEA} (-)	$N_{R.Cf}/N_{FEA}$ (-)
K3-S355	413.03	402.25	0.97	0.97
K3-S460	499.99	514.92	1.03	0.93
K3-S700	786.92	759.20	0.96	0.77
K3-S960	1061.02	1067.22	1.01	0.80
K4-S355	486.35	470.87	0.97	0.97
K4-S460	587.24	602.69	1.03	0.92
K4-S700	925.00	881.43	0.95	0.76
K4-S960	1223.20	1226.50	1.00	0.80
K5-S355	576.15	561.48	0.97	0.97
K5-S460	697.57	681.49	0.98	0.88
K5-S700	1092.94	999.57	0.91	0.73
K5-S960	1427.38	1407.28	0.99	0.79

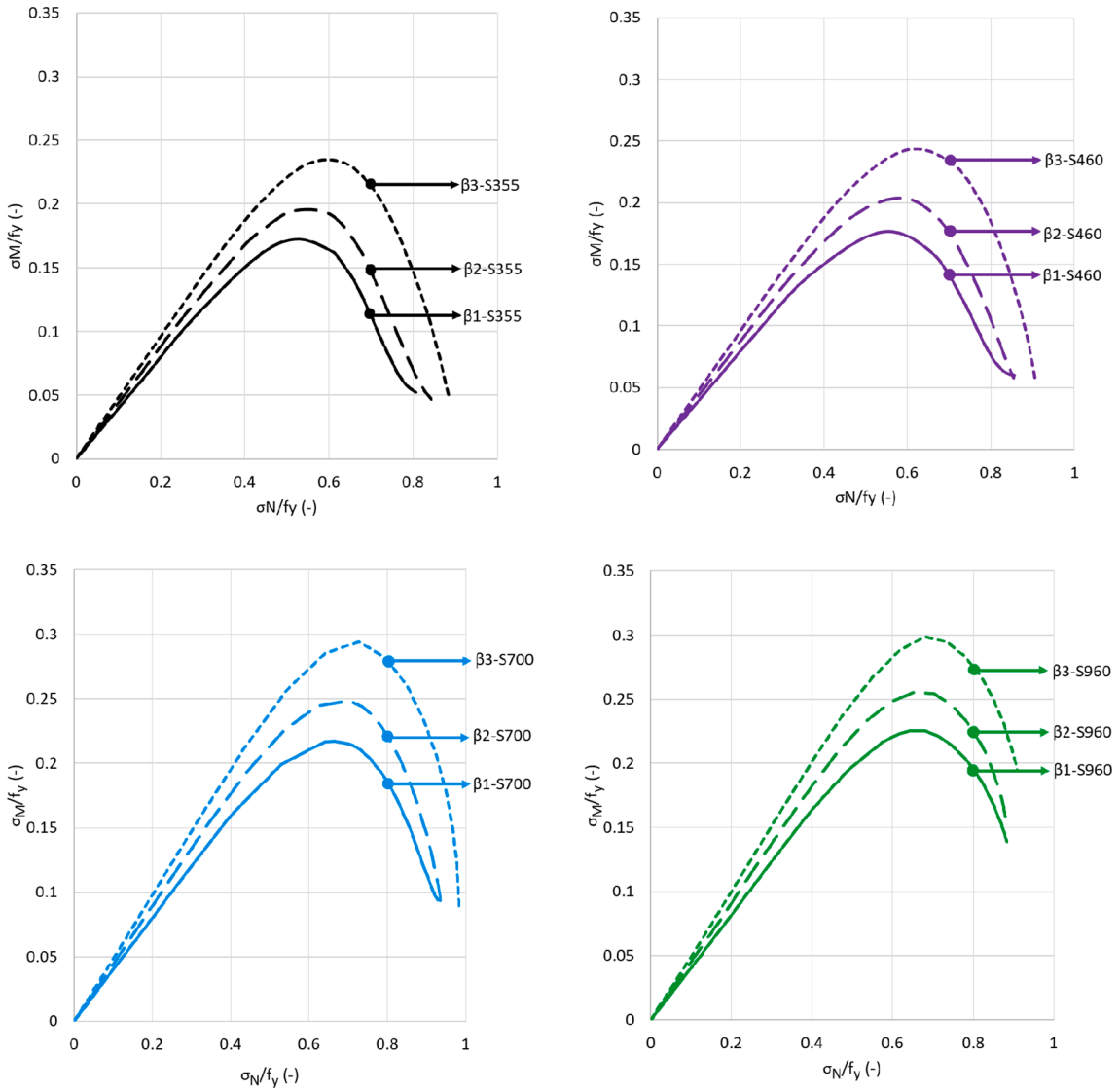

Fig. 14. Secondary bending stress with different β parameter for (a) S355, (b) S460, (c) S700 and (d) S960.

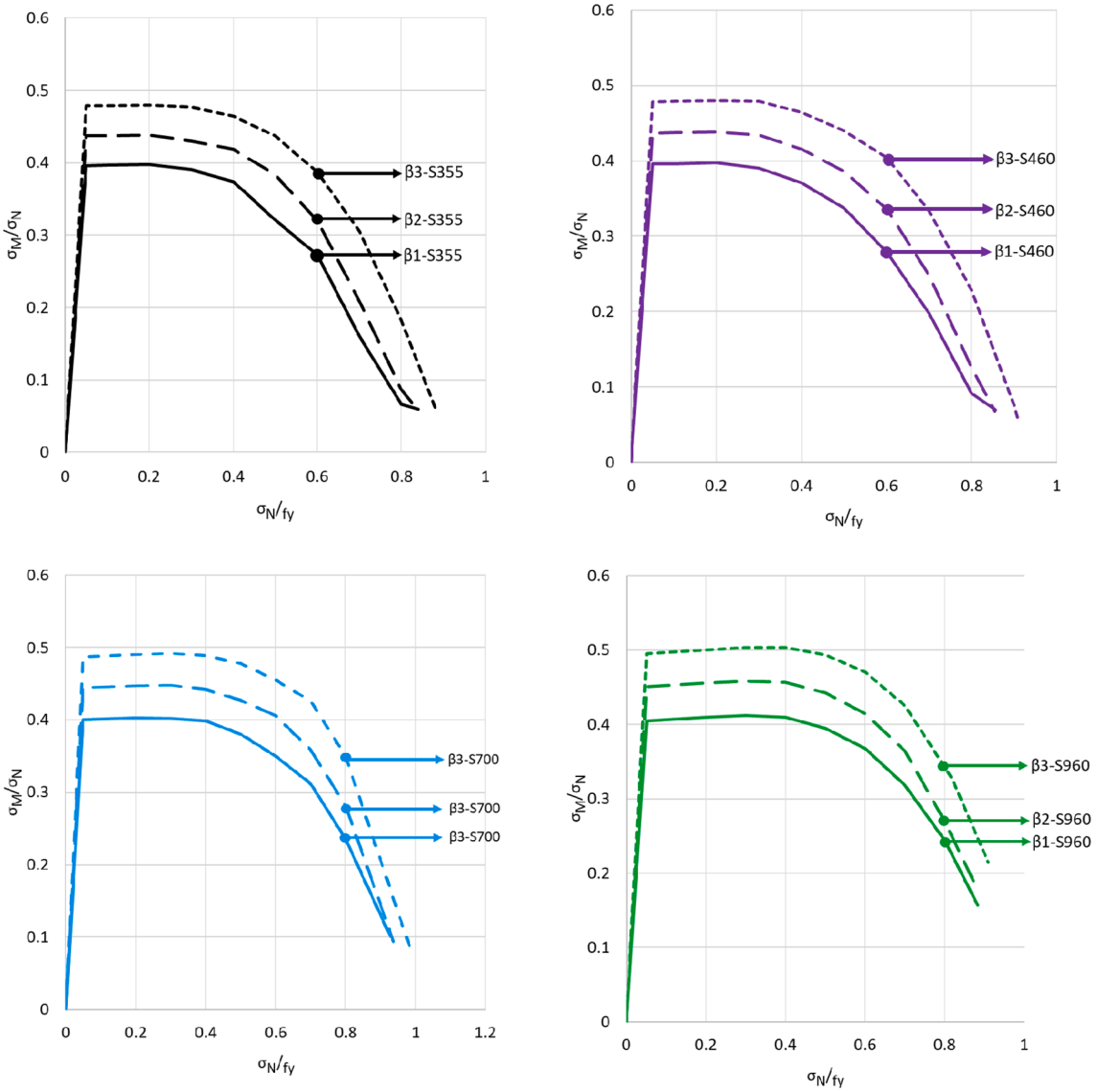

Fig. 15. Level of secondary bending stress with different β parameter for (a) S355, (b) S460, (c) S700 and (d) S960.

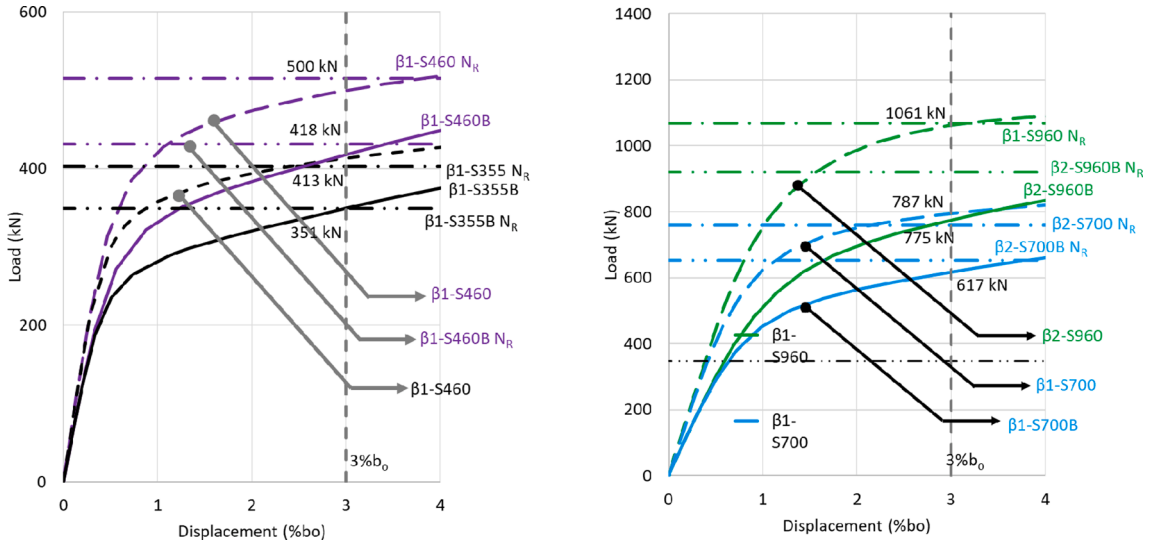

Fig. 16. Load displacement curve with different weld types for FE models with β_1.

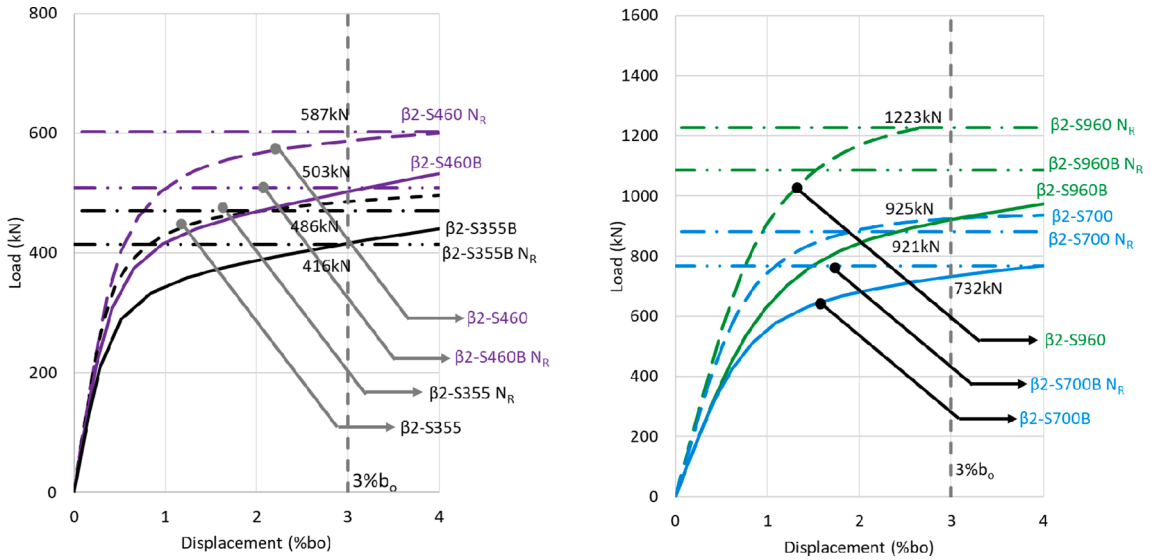

Fig. 17. Load displacement curve with different weld types for FE models with β_2.

internal work by the displacement of the chord face. As listed in Table 6, the joint resistance obtained by the yield line mechanism is 2%-16% lower compared to the ultimate load resistance obtained by the FEA.

5. Comparisons between fe results and design proposals

Fig. 24 shows material reduction factor C_f distribution for various steel grades. EN1993-1-8-DRAFT V4.2 recommended that $C_f = 1.0$ when $F_y \leq 355$ MPa, and $C_f = 0.9$ when $355 < F_y \leq 460$ MPa, and $C_f = 0.8$ when $460 < F_y \leq 700$ MPa. Based on the results presented in the paper, C_f is proposed as 1.0 when $F_y \leq 355$ MPa, 0.9 when $355 < F_y \leq 700$ MPa, and 0.8 when $700 < F_y \leq 960$ MPa. Note the assumption that material properties of welds and HAZ are same as the base material may affect the value of C_f. The values of reduction factor C_f need to be further improved.

6. Conclusion

A parametric study on the gap K joints is performed using "traditional" assumptions such as the same material properties for weld and base material and J2 plasticity model. Investigation of the material characteristics, gap size, the brace to chord width ratio and

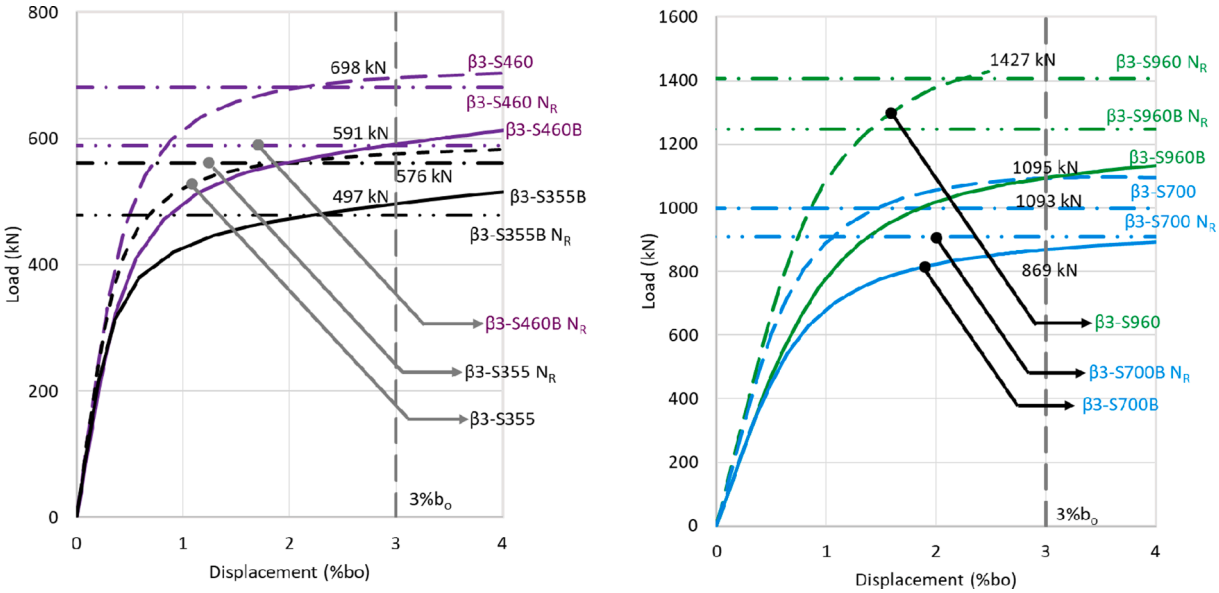

Fig. 18. Load displacement curve with different weld types for FE models with β_3.

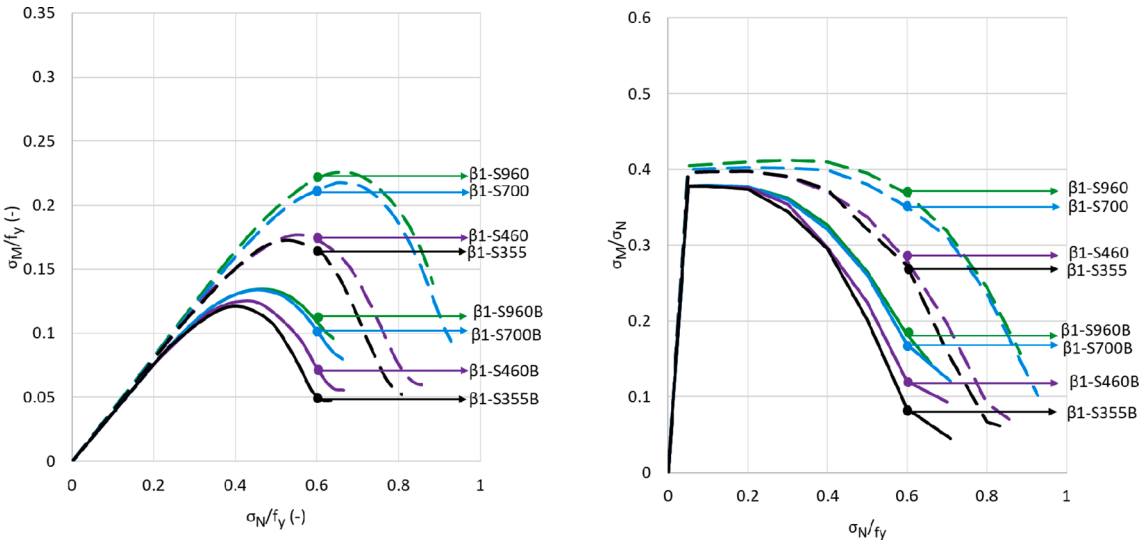

Fig. 19. Different weld type with β_1 (a) Secondary bending stress and (b) level of secondary bending stress.

welds type effects on the secondary bending stresses were performed and following could be emphasized:

(1) The secondary bending stress is larger for joints made of higher steel grades. The secondary bending stresses increases with increasing applied load but decreases later due to material softening. Note that the material models still need to be improved to better consider post necking behavior and multiaxial damage of the joints using HSS. These improvements may influence the ultimate resistance and failure mode. The material model used in this model underestimates the true stress magnitude after necking, and also did not consider the fracture effects. Joints with lower gap size, exhibit larger secondary bending stresses and lower ratio between secondary bending stress to average axial stress than joint with larger gap size.

(2) For each steel grade, larger β-values result in larger secondary bending stresses. Influence of the larger β-values for higher strength hollow section joints are lower when compared to mild-strength hollow section joints. For each steel grade, the secondary bending stresses in the fillet-welded joints are larger than that of the butt-welded joints.

(3) Based on the results presented in the paper, C_f is proposed 1.0 when $F_y \leq 355$ MPa, 0.9 when $355 < F_y \leq 700$ MPa, and 0.8 when $700 < F_y \leq 960$ MPa. Note that the material properties assumptions may affect the value of C_f. The values of reduction factor C_f

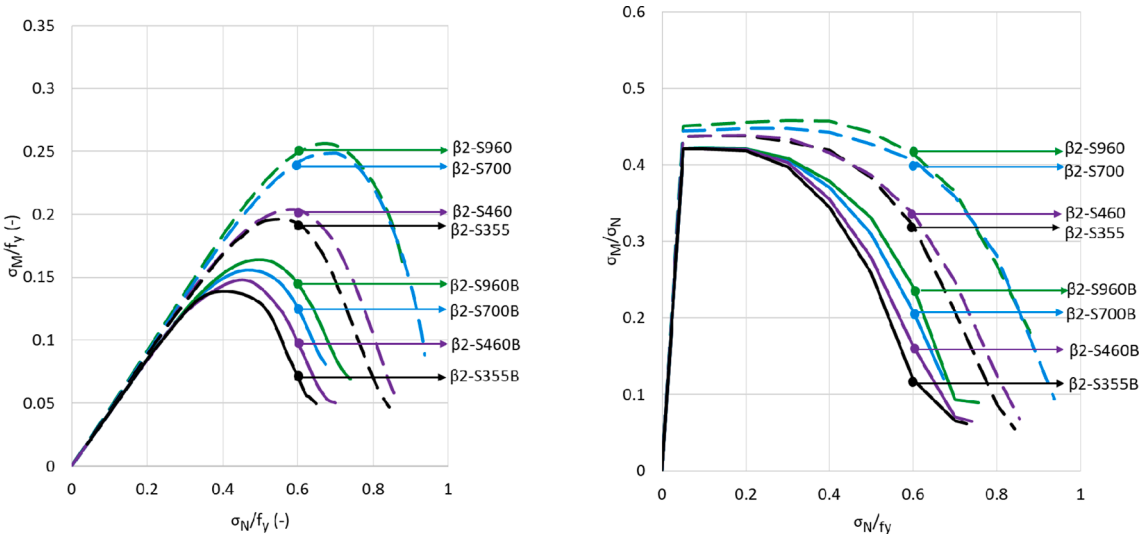

Fig. 20. Different weld type with β_2 (a) Secondary bending stress and (b) level of secondary bending stress.

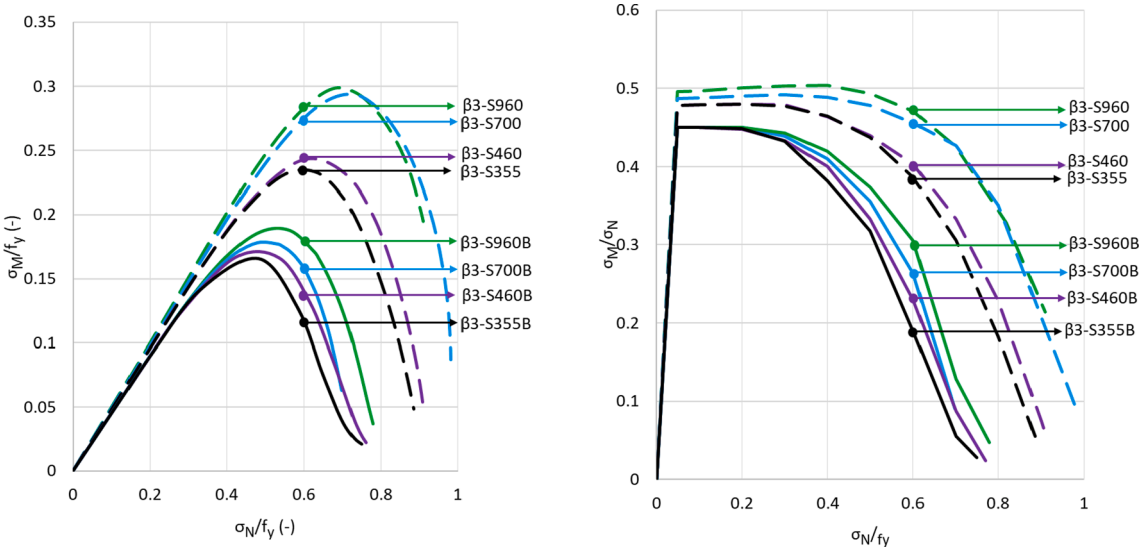

Fig. 21. Different weld type with β_3 (a) Secondary bending stress and (b) level of secondary bending stress.

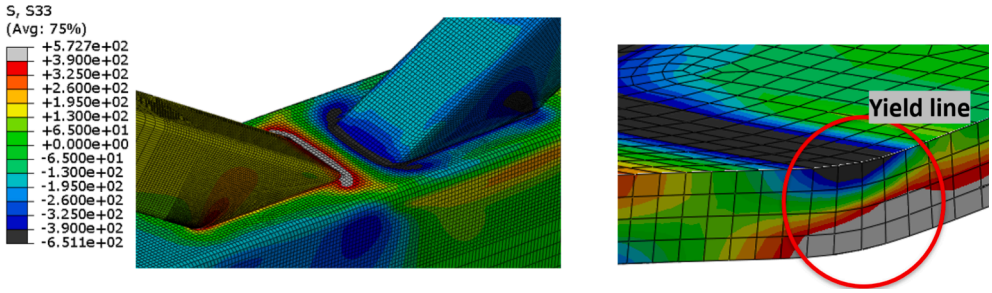

Fig. 22. Plastic moment at ultimate load resistance for K3 joints made of S355 materials.

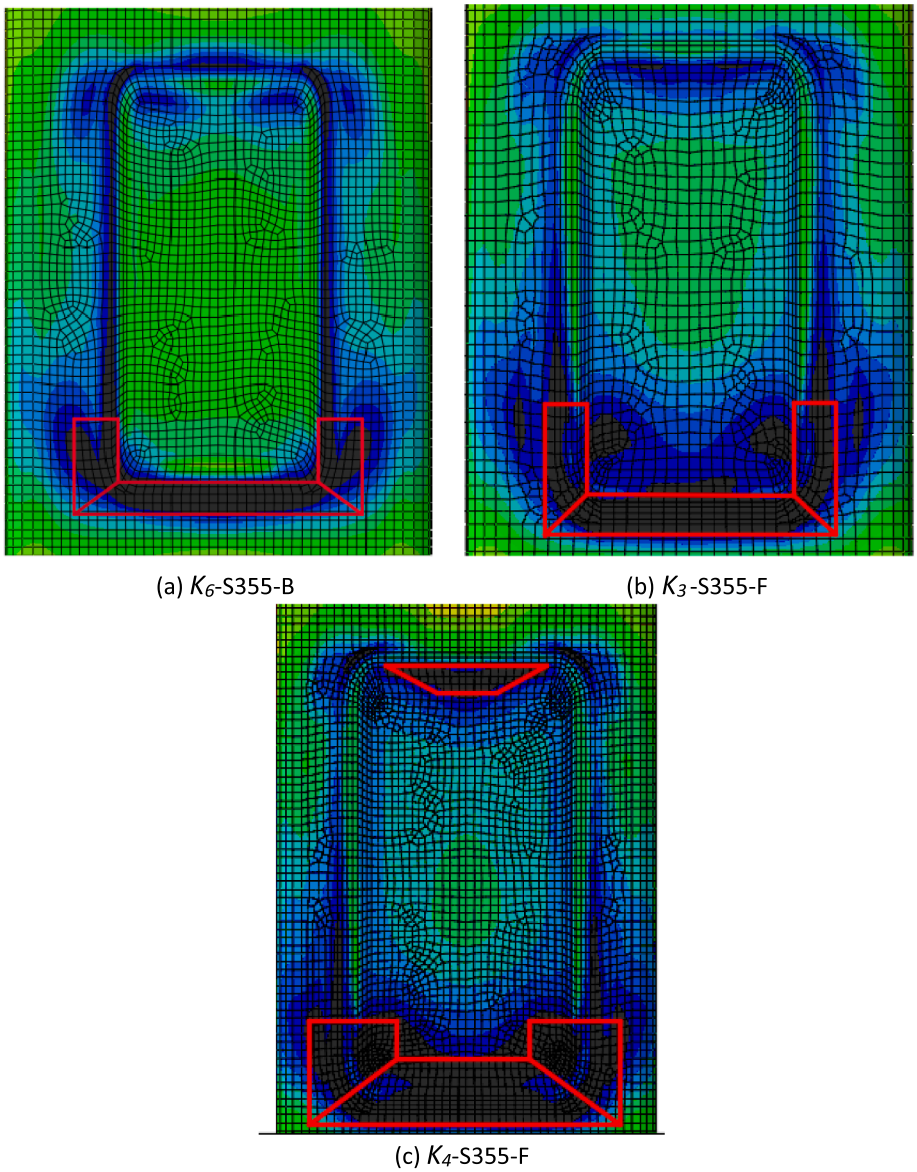

Fig. 23. Typical yiled line pattern of K-joints made of S355 materials.

Table 6
Resistance ratio between yield line methods and FE results (N_{YL}/N_{FEA}).

Model	Ultimate load resistance FEA N_{FEA}	Ultimate load resistance using yield lines N_{YL}	N_{YL}/N_{FEA}
	(kN)	(kN)	(-)
K_6-S355-B	351.16	319.28	0.91
K_6-S460-B	418.20	381.84	0.91
K_6-S700-B	629.60	552.46	0.88
K_6-S960-B	789.08	698.33	0.88
K_7-S355-B	420.20	432.54	0.91
K_7-S460-B	503.63	432.54	0.86
K_7-S700-B	730.79	661.93	0.91
K_7-S960-B	917.18	903.06	0.98
K_3 -S355-F	416.03	352.96	0.85
K_3-S460-F	416.03	383.61	0.92
K_3-S700-F	786.92	697.46	0.89
K_3-S960-F	1059.50	933.45	0.88
K_4-S355-F	486.3498	424.50	0.87
K_4-S460-F	586.8166	516.24	0.88
K_4-S700-F	926.1824	819.71	0.89
K_4-S960-F	1223.199	1030.74	0.84

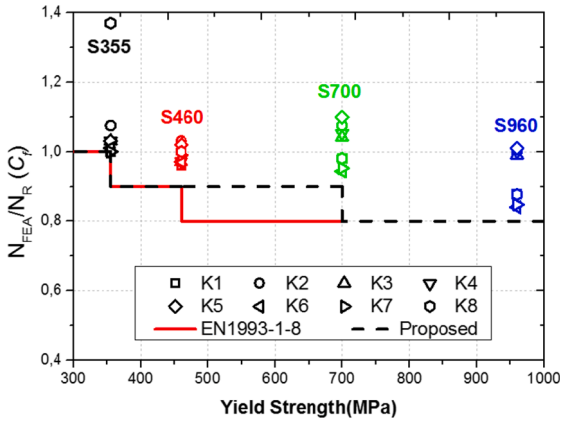

Fig. 24. Material reduction factor C_f distribution along yield strength.

will be further investigated by improved material models including distinction between HAZ, the filler material and base material.

Declaration of Competing Interest

The authors declare that they have no known competing financial interests or personal relationships that could have appeared to influence the work reported in this paper.

References

[1] M. Veljkovic, B. Johansson, Design of hybrid steel girders, J. Constr. Steel Res. 60 (2004) 535–547.
[2] H. Xin, J.A.F.O. Correia, M. Veljkovic, F. Berto, L. Manuel, Residual stress effects on fatigue life prediction using hardness measurements for butt-welded joints made of high strength steels, Int. J. Fatigue (2021) 106175.
[3] H. Xin, J.A.F.O. Correia, M. Veljkovic, F. Berto, Fracture parameters calibration and validation for the high strength steel based on the mesoscale failure index, Theor. Appl. Fract. Mech. 112 (2021).
[4] H. Xin, M. Veljkovic, J.A.F.O. Correia, F. Berto, Ductile fracture locus identification using mesoscale critical equivalent plastic strain, Fatigue Fract. Eng. Mater. Struct. (2021).
[5] H. Xin, J.A.F.O. Correia, M. Veljković, Three-dimensional fatigue crack propagation simulation using extended finite element methods for steel grades S355 and S690 considering mean stress effects, Eng. Struct. 227 (2021), 111414.
[6] M. Feldmann, N. Schillo, S. Schaffrath, K. Virdi, T. Björk, N. Tuominen, et al., Rules on High Strength Steel, Publ Off Eur Union Luxemb, 2016.
[7] J. Wardenier, J.A. Packer, X.-L. Zhao, G.J. Van der Vegte, Hollow Sections in Structural Applications, Bouwen met staal Rotterdam, The Netherlands, 2002.
[8] C.-H. Lee, S.-H. Kim, D.-H. Chung, D.-K. Kim, J.-W. Kim, Experimental and numerical study of cold-formed high-strength steel CHS X-joints, J. Struct. Eng. 143 (2017) 4017077.
[9] X. Lan, T.-M. Chan, B. Young, Static strength of high strength steel CHS X-joints under axial compression, J. Constr. Steel Res. 138 (2017) 369–379.
[10] X. Lan, T.-M. Chan, B. Young, Structural behaviour and design of chord plastification in high strength steel CHS X-joints, Constr. Build. Mater. 191 (2018) 1252–1267.

[13] J. Jiang, C.K. Lee, S.P. Chiew, Residual stress and stress concentration effect of high strength steel built-up box T-joints, J. Constr. Steel Res. 105 (2015) 164–173.
[14] S.P. Chiew, M.S. Zhao, C.K. Lee, Fatigue performance of high strength steel built-up box T-joints, J. Constr. Steel Res. 106 (2015) 296–310.
[15] Eurocode CEN. Design of steel structures—general rules—part 1–8: design of joints, EN1993-1-8: 2005 (E) 2005.
[16] T. Bjork, N.P.L.T. Tuominen, Effect of the secondary bending moment on K-joint capacity, in: Proc. 14th Int. Symp. Tubul. Struct., London, UK, 2015.
[17] Standardization. EN1993-1-8 v4.2 2018-07-27. Eurocode 3: Design of steel structures - Part 1-8: Design of joints. n.d.
[18] J. Wardenier, Y. Kurobane, J.A. Packer, G.J. van der Vegte XLZ. Design guide for circular hollow section (CHS) joints under predominantly static loading, CIDECT. Verlag TUV Rheinland, Col Ger 2008.
[19] M. Pavlovic, M. Veljkovic, Compact cross-sections of mild and high-strength steel hollow-section beams, Proc. Inst. Civ. Eng. Build. 170 (2017) 825–840.